A Novel Heat Shrinkable Ultrasonic Transducer for Rotary Ultrasonic Micro-Nano Precision Manufacturing

HENG ZHAO[1], SHUYUAN YE[1], JIANZHONG JU[1], ZHILI LONG[1], (Member, IEEE), AND YUHUI YANG[2]

[1]Department of Mechanical Engineering, Harbin Institute of Technology, Shenzhen 518055, China
[2]School of Electromechanical Engineering, Guangdong University of Technology, Guangzhou 510006, China

Corresponding author: Zhili Long (longzhili@hit.edu.cn)

ABSTRACT Rotary ultrasonic machining (RUM) has been proven to be a suitable technology for micro-nano precision manufacturing for hard and brittle ceramics/composite materials. However, the working frequency of the ultrasonic transducer in current RUM is in range from 20 kHz to 30 kHz. Moreover, the tool is tightened by an elastic chuck, which is in low clamping precision, high radial run-out, and unstable ultrasonic energy transmission. In this paper, we developed a novel heat shrinkable RUM ultrasonic transducer with 60 kHz frequency by equivalent circuit and finite element method (FEM). An analytical electromechanical equivalent circuit model was deduced to obtain the initial structure dimensions of the ultrasonic transducer. Three flange mounting structures were proposed to optimize and improve the energy transmission at the working resonant frequency. The influence of the proposed flanges on the resonant frequency of three transducers was analyzed and presented. The designed transducers were manufactured and tested in experiment. It shows that resonant frequencies of these three transducers with step, circular, and plate flange are 62.2 kHz, 61.46 kHz, and 61.4 kHz, and vibration amplitudes in 90 V driving voltage are $1.33 \mu m$, $4.74 \mu m$, $5.33 \mu m$, respectively. The working resonant frequencies by experimental measurement are consistent with the calculation result of the equivalent circuit and FEM. Moreover, the plate flange transducer shows the optimal amplitude capability with enough ultrasonic energy in micro-nano precision manufacturing.

INDEX TERMS Rotary ultrasonic machining, ultrasonic transducer, resonant frequency, equivalent circuit, finite element analysis.

I. INTRODUCTION

As an advanced special processing technology, rotary ultrasonic machining (RUM) has achieved good results in the processing of hard and brittle ceramic/composite materials, with high efficiency, lower cutting force and improved machining quality [1]–[6]. The technical principle of RUM is to apply auxiliary ultrasonic vibration on the tool in the processing of material removal. The ultrasonic transducer is driven and controlled by the ultrasonic generator, and then convert the high-frequency alternating current (AC)

The associate editor coordinating the review of this manuscript and approving it for publication was Yingxiang Liu.

electrical signals into mechanical vibration signals of the same frequency and amplify the vibration to the machining tool [7]–[9]. The frequency, impedance and phase characteristics of ultrasonic transducer have important effects on the amplitude energy and the machining quality of workpiece [10], [11]. It is well known that the typical structures of ultrasonic transducer include back slab, pre-tightening bolt, piezoelectric ceramic stack, ultrasonic amplifier, and machining tool [12], [13]. Currently, the vibration modes of ultrasonic transducer include longitudinal-bending vibration [14], longitudinal vibration [15], [16], radial amplified vibration [17], torsional vibration [18], longitudinal radial vibration [19], longitudinal torsional vibration [20], [21], etc.

With the increasing applications of the RUM in industry, academic researchers or engineers have adopted various methods to design, test and analyze ultrasonic transducer. Voronina and Babitsky used mass spring system to describe the dynamic characteristics of ultrasonic transducer under nonlinear contact load at resonant frequency [22], [23]. Wang et al. analyzed the dynamic characteristics of longitudinal piezoelectric transducer at its resonant frequency by using mass spring damping (MSD) [24]. Smyth and Kim designed a piezoelectric transducer for micro-manufacturing based on the Mason equivalent circuit [25]. Sammoura and Lin studied the relationship among the resonant frequency, mechanical load and displacement of the ultrasonic transducer by using the equivalent circuit of the four-terminal network [26]. Zhang et al. designed the ultrasonic transducer by using electromechanical equivalent circuit, and the optimized geometric model of the ultrasonic transducer was obtained by FEM and experimental test analysis [27]. For the frequency, impedance, phase characteristics of ultrasonic transducer, Wang et al. studied the general expressions of the applied load and resonant frequency of ultrasonic transducer by using numerical analysis [28]. Zhang et al. analyzed the characteristic changes in the conical horn at loading and summarized the relationship between the resonant frequency of the conical horn and the magnitude of loading [29]. In experiment, Zhao et al. investigated the tool load effect on the stability of the ultrasonic milling acoustic system based on the geometric parameters of the tool [30]. Ji et al. obtained the relationship between ultrasonic cutting force, system resonant frequency, and impedance by establishing the theoretical model of the ultrasonic cutting acoustic system [31]. Zhao et al. studied the influence of thermomechanical load on the vibration characteristics of ultrasonic vibration system [32].

In summary, longitudinal ultrasonic transducer is the typical structure applied in current RUM manufacturing. However, in longitudinal vibration machining, most researchers focused on the dynamic characteristics of ultrasonic transducer with external loading in material processing and the machining mechanism. Moreover, the mainstream working frequency of the current RUM is range from 20 kHz to 30 kHz, and higher working frequencies over 60 kHz are not reported till now. Moreover, for the conventional technique of tool mounting by an elastic chuck, the clamping precision is unstable, the radial run-out is in poor level, and the ultrasonic energy is in low transmission efficiency. In this paper, we developed a novel 60 kHz heat shrinkable ultrasonic transducer for RUM based on the equivalent circuit and finite element analysis. The initial geometrical structure of the transducer was attained by the numerical simulation. Then, three stiffness of proposed flanges were investigated, and its resonant frequencies and vibration modes for ultrasonic transducer are analyzed. Finally, the transducers were fabricated and the effects of the three flanges on resonant frequency, phase and impedance, amplitude characteristics were explored.
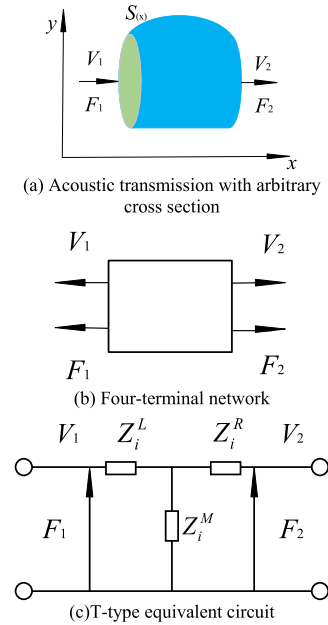

(a) Acoustic transmission with arbitrary cross section

(b) Four-terminal network

(c)T-type equivalent circuit

FIGURE 1. T-type equivalent circuit for four - terminal network of arbitrary section rod.
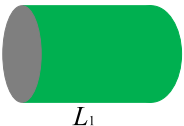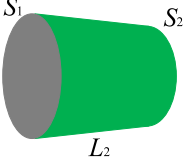
II. TRANSDUCER DESIGN

A. GEOMETRIC STRUCTURE DETERMINATION

As the media of ultrasonic transmission, a rod with any cross-section shape can be represented as a T-type equivalent circuit by the principle of acoustic-force-electrical analogy, as shown in Fig. 1. In Fig. 1 (a), V_1 and V_2 are the speed of terminal vibration; F_1 and F_2 are the terminal force; $S(x)$ is the function of the cross-section area of transmission rod. The mechanical force and velocity can be equivalent to a four-terminal network in Fig. 1 (b) and a T-type circuit in Fig. 1(c). Z_i^L, Z_i^R, Z_i^M are acoustic impedance of vibration denoted as the left, right and middle location of the T-type equivalent circuit, respectively. According to the equivalent feature between the acoustic-force-electrical analogies, we can attain the impedance expressions with cylinder and conical cross section rod in the equivalent circuit, as listed in Table 1. S is the area of constant rod. S_1 and S_2 are the area of conical rod end. L_1 and L_2 are the length of constant rod and conical horn. ρ, $c = \sqrt{E/\rho}$, $k = w/c$ are the density, sound speed, propagation constant of the material, and $w = 2\pi f$ is the angular frequency.

In this study, the basic configuration of ultrasonic transducer in RUM is designed as Fig. 2 (a), which consists of the piezoelectric ceramics, font and back plate, vibration amplified horn, and the machining tool. In this proposed transducer, the machining tool is clamped to the horn by the elastic deformation when the horn tip is expanded in high temperature and shrank in low temperature. Figure 2 (a) compares the difference between this novel clamping and the traditional clamping by an elastic chuck and nut/collet. It is well known that clamping by shrinkable force can achieve high connected precision and low radial run-out, which is beneficial to the

TABLE 1. Acoustic impedance expression correlated in theoretical analysis model.

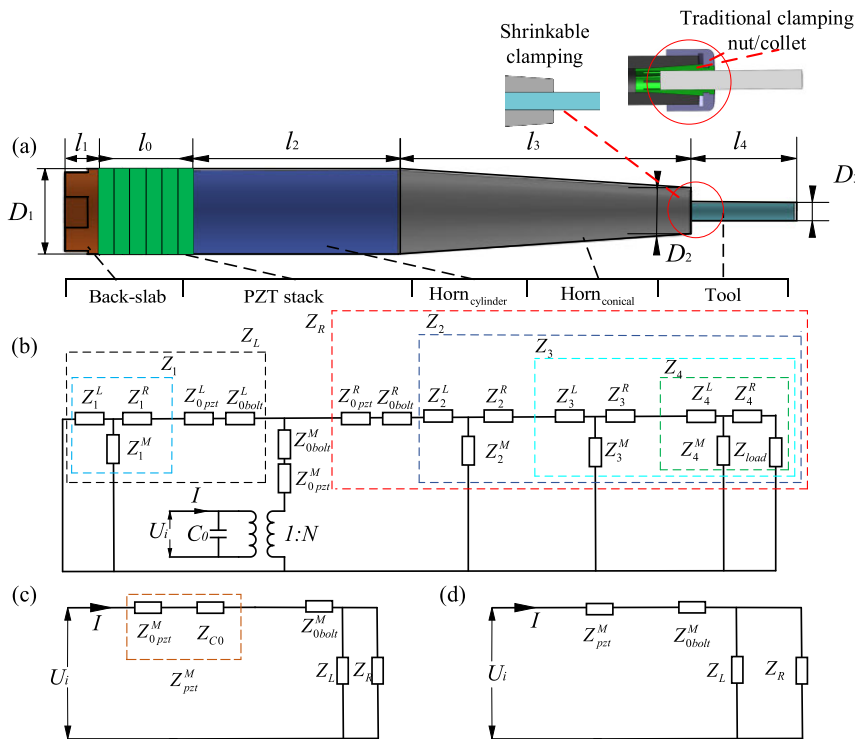| Type	Shape	Impedance expression
Cylindrical rod	S L_1	$Z_i^L = Z_i^R = j\rho c S \tan(kL_1 / 2)$ $Z_i^M = \dfrac{\rho c S}{j \sin(kL_1)}$
Conical rod	S_1 S_2 L_2	$Z_i^L = -j\rho c S_1(\sqrt{\dfrac{S_1}{S_2}} - 1) - j\rho c S_1 \cot(kL_2) - \dfrac{\rho c \sqrt{S_1 S_2}}{j \sin kL_2}$ $Z_i^R = \dfrac{\rho c \sqrt{S_1 S_2}}{j \sin(kL_2)}$ $Z_i^M = j\rho c S_2(1 - \sqrt{\dfrac{S_2}{S_1}}) - j\rho c S_2 \cot(kL_2) - \dfrac{\rho c \sqrt{S_1 S_2}}{j \sin kL_2}$

FIGURE 2. Equivalent circuit of ultrasonic transducer: (a) Structure of ultrasonic transducer;(b),(c), and (d). Equivalent circuit.

energy transmission. The ultrasonic transducer is identified with corresponding impedance in the equivalent circuit model shown in Fig. 2(b). Fig. 2(c) is the simplified circuit of Fig. 2(b), and Fig. 2(d) is the simplified circuit of Fig. 2(c). Z_1^L, Z_1^R, Z_1^M are the acoustic impedance of the back slab. Z_2^L, Z_2^R, Z_2^M are the acoustic impedance of the solid constant horn. Z_3^L, Z_3^R, Z_3^M are the acoustic impedance of the conical section of the solid horn. Z_4^L, Z_4^R, Z_4^M are the equivalent acoustic impedance of the clamping tool as the tool is approximately simplified as a cylinder. Z_{load} is the equivalent impedance of the external load at the end of tool, and $Z_{load} = 0$ as without load. Z_{0bolt}^L, Z_{0bolt}^R, and Z_{0bolt}^M are the equivalent

acoustic impedance of the pre-tightening bolt. Z_{0pzt}^L, Z_{0pzt}^R, and Z_{0pzt}^M are the acoustic impedance of the piezoelectric ceramic ring. Z_{pzt}^M is the equivalent acoustic impedance of piezoelectric ceramics. Z_L, Z_R are the equivalent impedance of the ultrasonic transducer at the left and right ends of the piezoelectric ceramic.

As to the piezoelectric ceramics in Fig. 2(b), Z_{C_0} is the equivalent impedance of the static capacitor C_0 [33], which can be expressed as

$$Z_{C0} = N^2/(jwC_0) \tag{1}$$

$$N = S_{pzt}d_{33}/(s_{33}^E h_{pzt}) \tag{2}$$

$$C_0 = nS_{pzt}\varepsilon_{33}^T(1 - k_{33}^2)/h_{pzt} \qquad (3)$$

where, N is the electromechanical conversion coefficient of piezoelectric ceramic stacks. S_{pzt} is the cross-sectional area. $d_{33} = 289 \times 10^{-12} \mathrm{CN}^{-1}$ is the piezoelectric strain constant. $s_{33}^E = 15.5 \times 10^{-12}\ \mathrm{m^2N^{-1}}$ is the elastic compliance constant. $h_{pzt} = 2.3$ mm is the thickness of piezoelectric ceramic. $n = 6$ is the numbers of piezoelectric ceramics. $\varepsilon_{33}^T = 1300\varepsilon_0$ is the dielectric constant and $\varepsilon_0 = 8.85 \times 10^{-12}\ \mathrm{Fm^{-1}}$. $k_{33} = 0.70$ is the electromechanical coupling coefficient. The equivalent impedance expression of Z_{pzt}^M is

$$Z_{pzt}^M = Z_{0pzt}^M - Z_{C0} \qquad (4)$$

The impedance on the left side of the piezoelectric ceramics is

$$Z_1 = Z_1^R + \frac{Z_1^L \times Z_1^M}{Z_1^L + Z_1^M} \qquad (5)$$

$$Z_L = Z_1 + Z_{0pzt}^L + Z_{0bolt}^L \qquad (6)$$

The impedance on the right side of the piezoelectric ceramics is

$$Z_4 = Z_4^L + \frac{Z_4^M \times (Z_4^R + Z_{load})}{Z_4^M + Z_4^R + Z_{load}} \qquad (7)$$

$$Z_3 = Z_3^L + \frac{Z_3^M \times (Z_3^R + Z_4)}{Z_3^M + Z_3^R + Z_4} \qquad (8)$$

$$Z_2 = Z_2^L + \frac{Z_2^M \times (Z_2^R + Z_3)}{Z_2^M + Z_2^R + Z_3} \qquad (9)$$

$$Z_R = Z_2 + Z_{0pzt}^R + Z_{0bolt}^R \qquad (10)$$

The impedance Z_R and Z_L are in parallel at the left and right side. Z_{pzt}^M, Z_{0bolt}^M are series impedance in the piezoelectric ceramics. Thus, the total impedance Z of the heat shrinkable ultrasonic transducer is expressed as

$$Z = \frac{1}{\gamma_a} = \frac{U}{I} = Z_{pzt}^M + Z_{0bolt}^M + \frac{Z_L \times Z_R}{Z_L + Z_R} \qquad (11)$$

$$\gamma_a = \frac{1}{Z} = \mathrm{Re}(\gamma_a) + \mathrm{Im}(\gamma_a) \qquad (12)$$

where, γ_a is the admittance. $\mathrm{Re}(\gamma_a)$ is the conductance of the admittance's real part. $\mathrm{Im}(\gamma_a)$ is the susceptance of admittance's imaginary part. The impedance and admittance model of the heat shrinkable ultrasonic transducer is expressed by the material characteristics, geometric dimension, natural resonant frequency, voltage and current parameters. When the acoustic impedance in model Z is in smallest value, the imaginary part $\mathrm{Im}(\gamma_a)$ of the admittance and the impedance phase angle are zero at the designated frequency, then the initial mechanical structure can be configured. The specific material properties and initial geometry parameters are shown in Table 2, when the resonant frequency of ultrasonic transducer is designated to 60 kHz frequency.

TABLE 2. Parameters of the transducer.

Part	Material	Density (kg. m⁻³)	Poisson ratio	Young modulus (GPa)	Diameter (mm)	Length (mm)
PZT stack l_0	PZT-4	7500	0.31	64.5	15	14
Backplate l_1					15	6
Constant horn l_2	Stainless steel	7850	0.30	215	15	36
Conical horn l_3					S₁:15 S₂:8	51
Tool l_4					3.175	18

B. FREQUENCY AND IMPEDANCE CHARACTERISTIC

Based on above equivalent circuit, the impedance-phase and conductance-susceptance are attained when we sweep the frequency in range from 10kHz to 100kHz, and the results are shown in Fig. (3). In Fig. 3(a) and (c), there are multiple resonant frequencies, where the first, second, third and fourth frequency are 21.4 kHz, 36.23 kHz, 60.35 kHz, 86.68 kHz, respectively. Specifically, in Fig. 3(b), at the third mode frequency of 60.35 kHz, the impedance reaches its lowest value and conductance reaches to the peak point. In addition, the phase and susceptance also reach to zero in Fig. 3(d) at the 60.35 kHz frequency. Thus, the frequency by equivalent circuit is in good agreement with the designed 60 kHz frequency.

C. INFLUENCE OF GEOMETRIC DIMENSION ON IMPEDANCE AND FREQUENCY

As shown in Fig. 4, the influence of the geometric dimensions on the frequency and impedance of the ultrasonic transducer was calculated numerically based on the impedance model. It can be found that the impedance increases and the frequency decreases as the back-slab thickness l_1 turns high. As the horn length l_2 of the cylindrical section, the horn length l_3 of the cone section and the diameter D_2 of the clamping end for the tool turns short, the impedance and resonant frequencies decreased. Based on this approach, we can determine the structure dimensions of the 60 kHz resonant frequency of the ultrasonic transducer by adjusting mutually the corresponding geometric structures.

III. STRUCTURAL OPTIMIZATION
A. MODAL ANALYSIS

In RUM system, the heat shrinkable ultrasonic transducer is located and fastened by the flange structure in the spindle. In order to improve the ultrasonic vibration, the mounting flange should be located at the vibration node. In this paper, we adopted ANSYS APDL software to analyze the dynamic characteristics of the ultrasonic transducer by modal analysis. The material properties are shown in Table 2. The transducer assembly is meshed with 61532 nodes, and the vibration frequency and modes are obtained by Block Lanczos solver. Fig. 5 shows the four longitudinal modes in frequency from 10 kHz to 100 kHz, and the third mode is concerned as the working vibration in the material removing. Table 3 lists
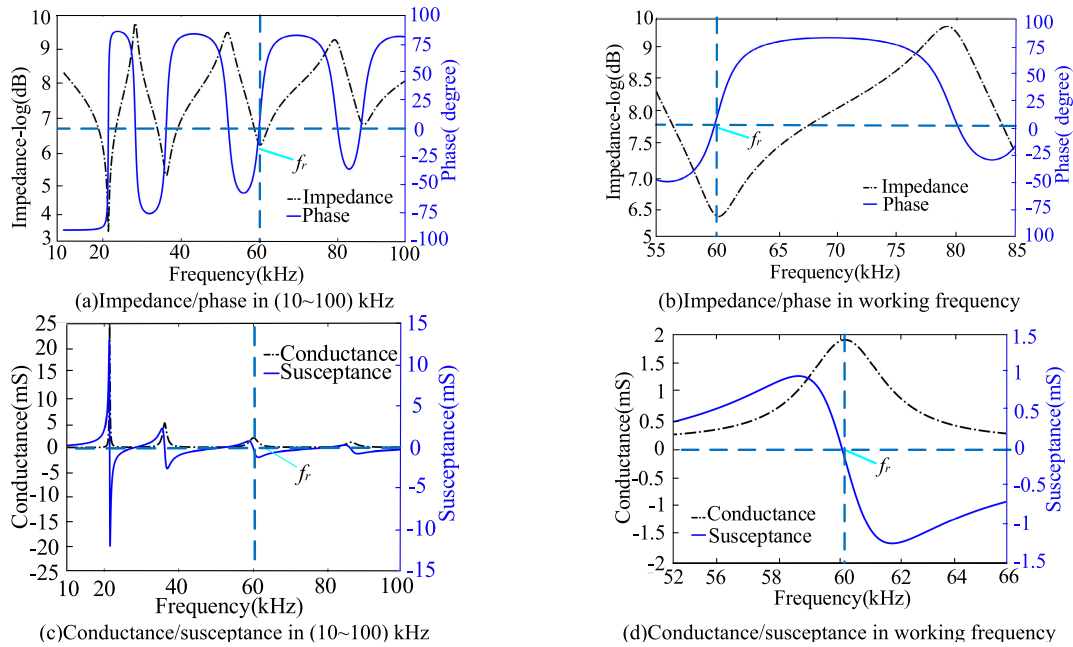
(a)Impedance/phase in (10~100) kHz

(b)Impedance/phase in working frequency

(c)Conductance/susceptance in (10~100) kHz

(d)Conductance/susceptance in working frequency

FIGURE 3. Dynamic characteristics of ultrasonic transducer.

(a)Thickness of back slab

(b)Length of solid horn cylinder section

(c)Length of solid horn cone section

(d)Outer diameter of clamping end
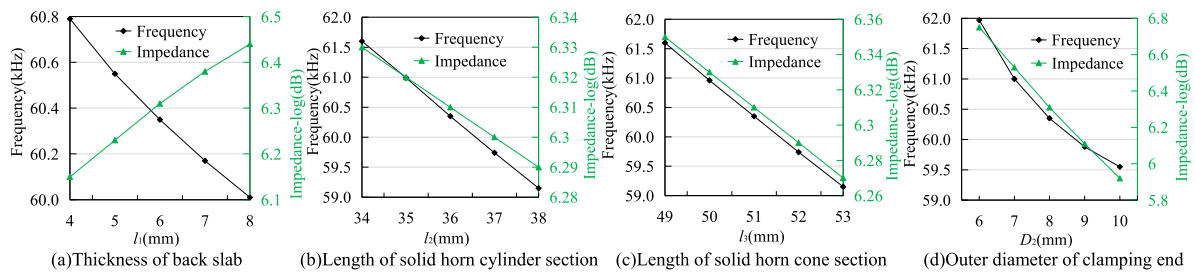
FIGURE 4. The influence of geometric dimension on impedance and frequency.

(a)25.65kHz
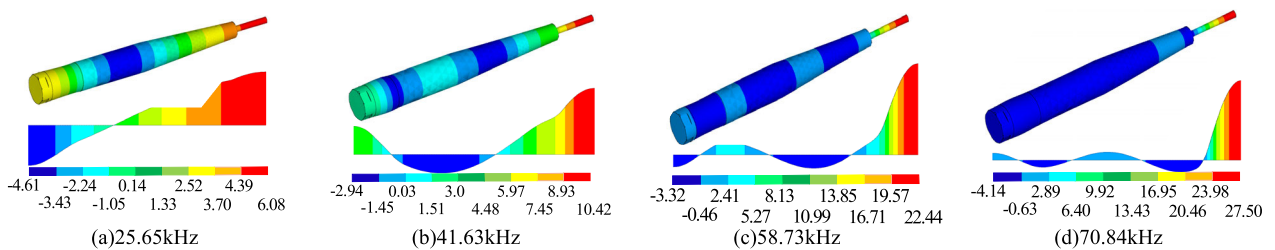
(b)41.63kHz

(c)58.73kHz

(d)70.84kHz

FIGURE 5. Modal analysis.

the errors of resonant frequencies between the equivalent circuit and FEM simulation. It is found that the third resonant frequency of FEM is 58.73 kHz, and the error is less than 3%, which is consistent with numerical result of 60.35 kHz. Large errors appear in the first, second and fourth longitudinal frequency between numerical simulation and FEM result, because the structure dimensions of the ultrasonic transducer is determined by the third resonant frequency from the equivalent circuit model. The mode shapes in the X, Y and Z

directions of the third mode for the ultrasonic transducer are shown in Fig. 6, where Y is the longitudinal vibration mode, and X, Z are the orthogonal non-longitudinal modes. The longitudinal mode of ultrasonic transducer shows a relatively large amplitude, and non-longitudinal displacements of X and Z direction vibration are not 0, which indicates that the total vibration mode of ultrasonic transducer is integrated by the coupling of displacement vectors in multiple directions. According to the third longitudinal vibration mode in Fig. 6,

TABLE 3. Comparison of numerical analysis and FEM.

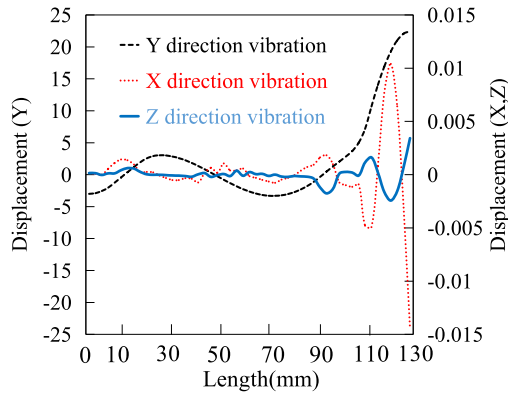| Mode	First	Second	Third	Fourth
Numerical (kHz)	21.40	36.23	60.35	86.68
FEM (kHz)	25.65	41.63	58.73	70.84
Error (%)	19.85	14.15	2.76	15.84

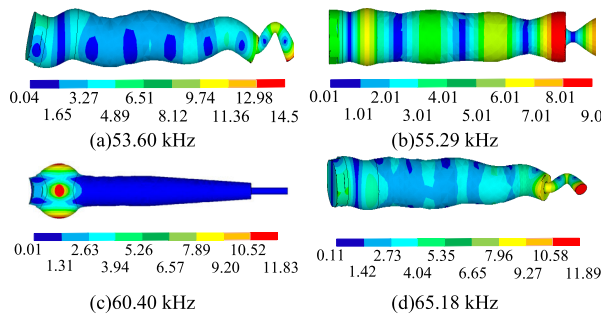**FIGURE 6.** Vibration mode at working frequency.

FIGURE 7. Vibration modes near to the working frequency.

the vibration node is located at 50 mm on the horn, which is selected as the flange clamping location. From FEM result, we find that multiple vibration modes are near to the operating frequency of 58.73 kHz, as shown in Fig. 7. These modal vibrations include composite bending and torsion (53.60 kHz, 65.18 kHz), lateral expansion and contraction (55.29 kHz), distortion in piezoelectric ceramic stack (60.40 kHz). As the ultrasonic transducer is excited close to these non-axial modal frequencies by ultrasonic generator, ultrasonic vibration energy would be decreased or unstable. Therefore, it is necessary to optimize the working resonant frequency to deviate away from these non-axial modal frequencies, achieving to improve the longitudinal vibration performance.

B. OPTIMIZATION FOR MOUNTING STRUCTURE

It is known that the ultrasonic transducer is connected to the spindle holder on the node location by a flange structure. As the working resonant frequency shifts far from resonant longitudinal frequency, the vibration node is not the accurate nodal location, which will reduce the ultrasonic vibration

amplitude. Moreover, the flange structure would inevitably affect the vibration characteristics, including the shift of resonant frequency, and the vibration deformation. It is important to adopt appropriate flange structure to maintain high ultrasonic amplitude.

TABLE 4. Structure dimensions of three flanges.

Structure parameter	r_1	r_2	r_3	l_1	l_2	l_3	l_5	l_6
Value(mm)	7.5	16	14	4.5	7	1.5	3	2.5

We proposed three flange structures for the ultrasonic transducer, including step, circle and plate flange, as shown in Fig. 8. The geometric dimensions are listed in Table 4. The part area of flange connected with the shank handle is regarded as the fixed support, and the part connected to the solid horn of the transducer is the loaded area. Thus, the flange cross-section in y direction is equivalent to a cantilever beam, and the flange stiffness is investigated by the deformation under an identical load. The cantilever beam shapes of three flange structures are expressed as

$$y_{\text{step}} = l_2 \ (0 \le x < l_1) \tag{13}$$

$$y_{\text{circle}} = \begin{cases} l_3 \ (0 \le x < l_6) \\ l_2 \ (l_6 \le x < l_1) \end{cases} \tag{14}$$

$$y_{\text{plate}} = l_3 \ (0 \le x < l_4) \tag{15}$$

where, l_1, l_2, l_3 and l_4 are structural dimensions of the flange cross-section. F_y is the applied load. The maximum loaded displacement of the flange can be expressed as

$$\Delta = \frac{1}{2} \int_0^l \frac{F_y(l-x)}{EI_z} dx \tag{16}$$

where, EI_z is the bending stiffness; E is Young's modulus; I_z is moment of inertia, which is expressed as

$$I_z = d_z \times y^3(x)/12 \tag{17}$$

where, d_z is the thickness of cantilever beam section, and d_z is the same in these three flanges. Therefore, the deformation in y direction of three flanges are deduced as

$$\Delta_{\text{step}} = \frac{v^1 y}{EI_2^3} \int_0^4 (l_1 - x) \, dx$$
$$= \frac{6F_y}{EI_2^3} \int_0^{l_6} (l_1 - x) \, dx + \frac{6F_y}{EI_2^3} \int_{l_6}^{l_1} (l_1 - x) \, dx \tag{18}$$

$$\Delta_{\text{circle}} = \frac{6F_y}{EI_3^3} \int_0^{l_6} (l_1 - x) \, dx + \frac{6F_y}{EI_2^3} \int_{l_6}^{l_1} (l_1 - x) \, dx$$

$$\Delta_{\text{plate}} = \frac{6F_y}{EI_3^3} \int_0^{l_1} (l_1 - x) \, dx \tag{19}$$
$$= \frac{6F_y}{EI_3^3} \int_0^{l_6} (l_1 - x) \, dx + \frac{6F_y}{EI_3^3} \int_{l_6}^{l_4} (l_1 - x) \, dx \tag{20}$$
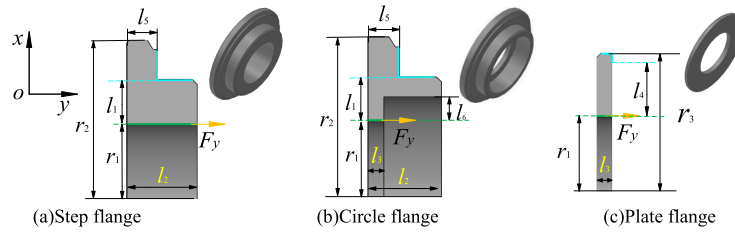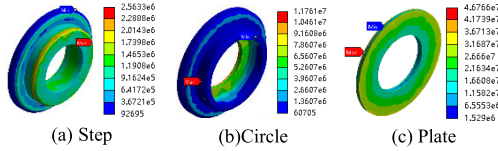
FIGURE 8. Mounting flanges.
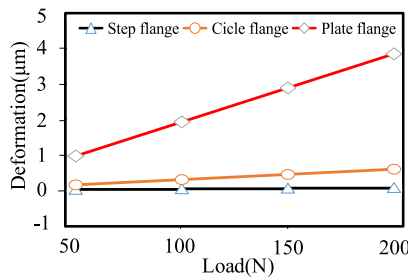

FIGURE 9. Stress of flange under 200N load.
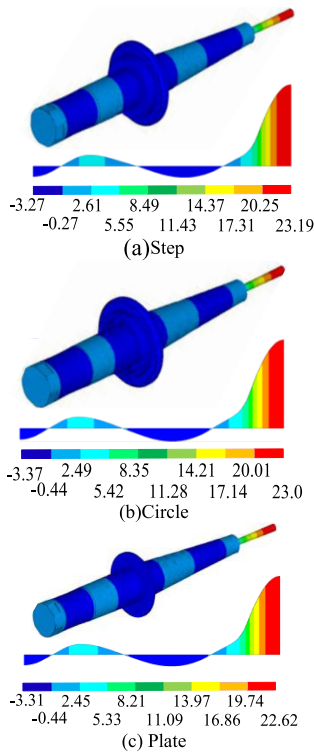

FIGURE 10. Deformation of flange with increasing load.

FIGURE 11. Vibration modes for three mounting flanges.

When $l_2 > l_3$, it can be concluded that $\Delta_{\text{circle}} > \Delta_{\text{step}}$ from (18) and (19). Similarly, $\Delta_{\text{plate}} > \Delta_{\text{circle}}$ as $l_1 = l_4$. Thus, we can affirm that the deformation under the same load
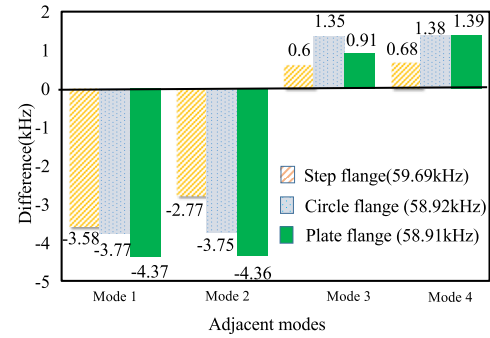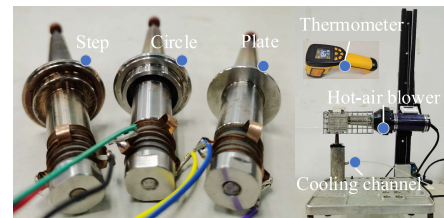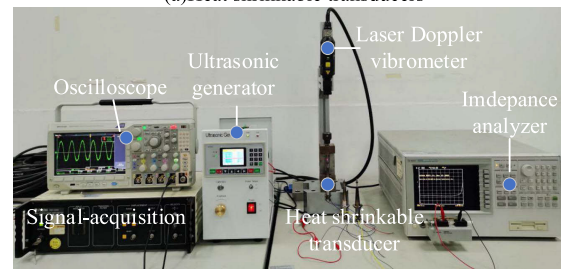

FIGURE 12. Frequency shift of three flange transducers.

FIGURE 13. Experiment setup.

of three flanges is

$$\Delta_{\text{plate}} > \Delta_{\text{circle}} > \Delta_{\text{step}} \qquad (21)$$

Meanwhile, we verified the deformation of the three flanges by FEM, and the result is shown in Fig. 9. It finds that the equivalent stress of the plate flange is maximal under 200N load, which is less than the material yield stress 355MPa, indicating that three designed flanges are reliable. The deformations of the three flanges are compared in Fig. 10, which shows that the deformation of plate flange is higher than the other two flanges when the load turns up. The largest deformation of plate flange is less than 5μm. Thus, it can be inferred from (21) and Fig. 10 that the plate flange
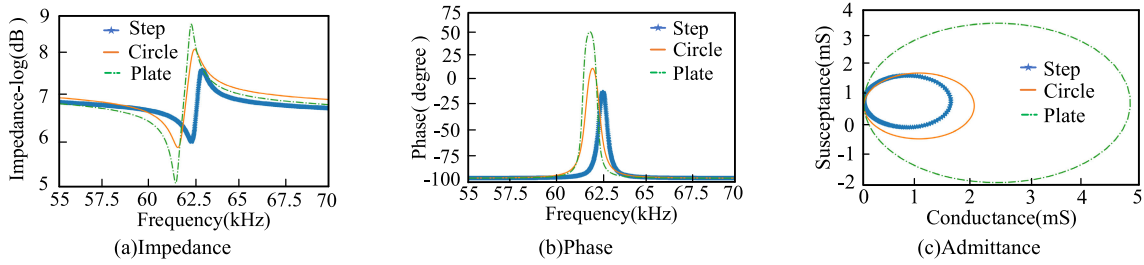
FIGURE 14. The impedance, phase, admittance characteristics of three ultrasonic transducers.
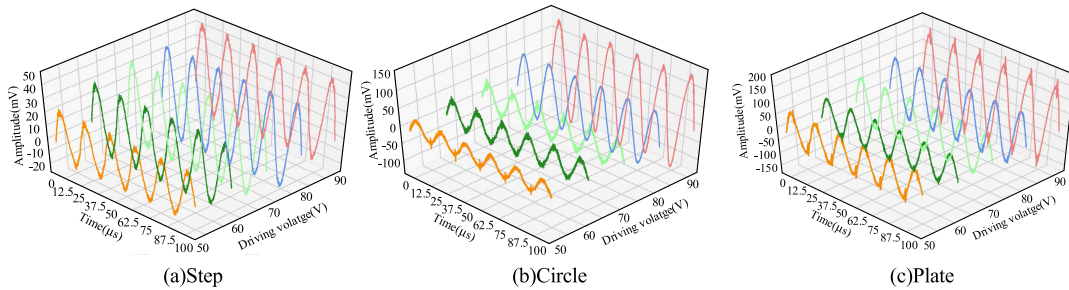

FIGURE 15. Amplitude of the ultrasonic transducer with three flanges.

has the lowest stiffness and the stepped one has the largest stiffness.

Figure 11 demonstrates the modal vibration of ultrasonic transducer with these three flanges. It is found that the resonant frequencies of step, circle, and plate flange are 59.69kHz, 58.92kHz, 58.91kHz, respectively. The longitudinal resonant frequency of ultrasonic transducer increases with the stiffness of the mounting flange. The resonant frequency of plate flange transducer is closest to initial one, meaning that the working frequency and vibration node is not shifted obviously.

Four non-axial modal frequencies near to working resonant frequency for the transducer with three flanges are obtained in Fig. 12. In the figure, modes 1 and 2 are the two non-axial mode frequencies lower to the resonant one; modes 3 and 4 are the two ones higher to the resonant frequency. It can be found that the working frequency of the plate flange transducer in non-axial vibration is in largest drifting, which means the highest robustness in the ultrasonic vibration. Therefore, the optimized clamping of ultrasonic transducer is the plate flange with appropriate stiffness among these three proposed flange structures.

IV. EXPERIMENTAL TESTS

The ultrasonic transducer prototype was manufactured, assembled and tested. Figure 13 shows the experimental platform, which includes the assembled transducer, hot-air blower machine for heat shrinkable tool clamping, thermometer, Agilent H4294A analyzer testing for frequency, impedance, and phase, self-developed ultrasonic generator, Tektronix Oscilloscope for voltage or current acquisition,

HSV 700 Laser Doppler Vibrometer for amplitude measurement. The experiment of machining tool clamping to the horn was carried out by a hot-air blower, as shown in Fig. 13(a). The tool was successfully clamped in the ultrasonic transducer, as the temperature was less than 200 °C when the whole body of the transducer is in cooling, which ensure that the piezoelectric ceramics is in a normal performance [33]. The ultrasonic transducers are fixed at its node location by a vice plain in our testing.

TABLE 5. Resonant frequency of designed transducer in experiment.

Type	Step	Circle	Plate
Frequency(kHz)	62.2	61.46	61.4

A. IMEPEDANCE MEASUREMENT

Table 5 lists the working resonant frequencies of these three ultrasonic transducers as the driving frequency is swept from 55 kHz to 70 kHz. Figure 14 demonstrates the frequency, impedance, phase, and admittance characteristics of these three ultrasonic transducers. The experimental measurement shows that the resonant frequencies of three ultrasonic transducers are coincide with the ones of the equivalent circuit and the FEM, where the error is less than 5%. In Fig. 14 (a), the impedance-frequency curve of the plate flange transducer is in the lowest impedance at resonant frequency comparing to the other two transducers, meaning that the plate flange transducer can vibrate in a higher energy under the same driving voltage. Fig. 14 (b) illustrates that the phase of step flange transducer cannot exceed to zero at its resonant frequency. Since the phase cannot reach zero, reactive power loss would

happen to the step flange transducer at the driving frequency, which vibrates in low amplitude. On the contrary, the phase of the circle and plate flange transducer can reach to zero, so their equivalent circuit can be regarded as a pure resistance to achieve higher mechanical and electrical energy transfer efficiency at the zero phase. Compared with the stepped and circle flange ultrasonic transducer, the admittance circle area of the plate flange ultrasonic transducer is the largest, indicating that it shows the ability of highest vibration and robustness under the same driving voltage.

B. AMPLITUDE MEASUREMENT

The amplitude waveforms of the machining tool in stable state at different driving voltages are shown in Fig. 15. The calibrated amplitude is shown in Fig. 16, showing that the amplitude of the machining tool tip increases with the voltage. The maximum amplitudes of three ultrasonic transducers are $1.33 \mu m$, $4.74 \mu m$, and $5.33 \mu m$, respectively. The vibration of the plate flange transducer shows the largest vibration amplitude under the same driving voltage, which confirms the correctness of the theoretical analysis and FEM calculation. The plate flange transducer with appropriate stiffness mounted at the vibration node, can produce the highest vibration among three flange transducers. Moreover, the maximum amplitude of the plate flange transducer is more than $5 \mu m$ with the 60 kHz high working frequency, indicating that it owns enough ultrasonic energy in micro-nano precision manufacturing.
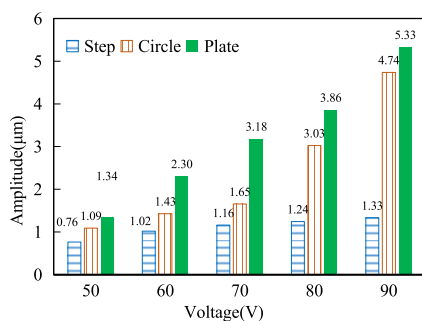

FIGURE 16. The calibrated amplitude of three ultrasonic transducers.

V. CONCLUSION

In the hard and brittle material precision manufacturing, RUM is an effective solution while this technology needs to be improved for more accuracy and higher efficiency. In our study, a novel heat shrinkable 60 kHz transducer for RUM was developed and verified in experiment.

The initial dimensions of the ultrasonic transducer were attained by the electromechanical equivalent circuit model. In order to improve the vibration energy at the resonant frequency, we proposed three flange structures to mount the transducers. The influence of flange structures on the resonant frequency and vibration was analyzed by theoretical analysis and FEM. Three flange transducers were

manufactured and measured in experiment. The resonant frequencies of the circle, step and plate flange transducers are 62.2 kHz, 61.46 kHz, and 61.4 kHz, and their maximum amplitudes are $1.33 \mu m$, $4.74 \mu m$, $5.33 \mu m$, respectively. Experimental results show that the resonant frequencies of the ultrasonic transducers are consistent with the theoretical modeling. The frequency trend coincides with the stiffness of flanges. Plate flange transducer can generate the largest amplitude and sufficient ultrasonic power in engineering application. This novel heat shrinkable transducer shows the potential feasibility to improve the machining quality in micro-nano precision manufacturing.
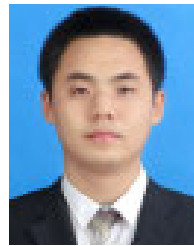
REFERENCES

[1] M. Baraheni and S. Amini, "Predicting subsurface damage in silicon nitride ceramics subjected to rotary ultrasonic assisted face grinding," *Ceram. Int.*, vol. 45, no. 8, pp. 10086–10096, Jun. 2019.

[2] D. Geng, Y. Liu, Z. Shao, Z. Lu, J. Cai, X. Li, X. Jiang, and D. Zhang, "Delamination formation, evaluation and suppression during drilling of composite laminates: A review," *Compos. Struct.*, vol. 216, pp. 168–186, May 2019.

[3] S. Yuan, H. Fan, M. Amin, C. Zhang, and M. Guo, "A cutting force prediction dynamic model for side milling of ceramic matrix composites C/SiC based on rotary ultrasonic machining," *Int. J. Adv. Manuf. Technol.*, vol. 86, nos. 1–4, pp. 37–48, Sep. 2016.

[4] Y. Cao, "Failure analysis of exit edges in ceramic machining using finite element analysis," *Eng. Failure Anal.*, vol. 8, no. 4, pp. 325–338, Aug. 2001.

[5] Z. Shao, X. Jiang, D. Geng, Y. Yang, Z. Peng, S. Li, and D. Zhang, "Deep hole drilling of large-diameter titanium alloy with a novel rotary low-frequency vibration device," *IEEE Access*, vol. 7, pp. 154872–154881, 2019.

[6] G. Qiao, M. Zhou, and M. Wang, "Study on surface roughness in ultrasonic vibration mill-grinding of hot-pressed Si_3N_4," *Int. J. Abrasive Tech.*, vol. 5, no. 2, pp. 175–186, 2012.

[7] X. Jiang, K. Wang, R. Shao, J. K. Mills, and D. Zhang, "Self-compensation theory and design of contactless energy transfer and vibration system for rotary ultrasonic machining," *IEEE Trans. Power Electron.*, vol. 33, no. 10, pp. 8650–8660, Oct. 2018.

[8] Z. Liu, Y. H. Jin, P. Bian, and B. Zhao, "Study on influence of load on characteristics of ultrasonic machining acoustic system," *Aviation Precis. Manuf. Technol.*, vol. 48, no. 1, pp. 10–13, 2012.

[9] B. Zhao, B. Chang, L. Yuan, and P. Li, "Influence of force load on the stability of ultrasonic longitudinal–torsional composite drilling system," *Int. J. Adv. Manuf. Technol.*, vol. 106, nos. 3–4, pp. 891–905, Jan. 2020.

[10] Z. Shao, Z. Li, and D. Zhang, "Study on the thrust force and chip in rotary ultrasonic-assisted drilling of titanium alloys (Ti_6Al_4V)," *J. Mech. Eng*, vol. 53, no. 19, pp. 66–72, 2017.

[11] K.-L. Kuo, "Design of rotary ultrasonic milling tool using FEM simulation," *J. Mater. Process. Technol.*, vol. 201, nos. 1–3, pp. 48–52, May 2008.

[12] A. Abdullah and A. Pak, "Correct prediction of the vibration behavior of a high power ultrasonic transducer by FEM simulation," *Int. J. Adv. Manuf. Technol.*, vol. 39, nos. 1–2, pp. 21–28, Oct. 2008.

[13] Z. Long, Y. Wu, L. Han, and J. Zhong, "Dynamics of ultrasonic transducer system for thermosonic flip chip bonding," *IEEE Trans. Compon. Packag. Technol.*, vol. 32, no. 2, pp. 261–267, Jun. 2009.

[14] X. Tang, Y. Liu, S. Shi, W. Chen, and X. Qi, "Development of a novel ultrasonic drill using longitudinal-bending hybrid mode," *IEEE Access*, vol. 5, pp. 7362–7370, 2017.

[15] S. Lin, H. Guo, and J. Xu, "Actively adjustable step-type ultrasonic horns in longitudinal vibration," *J. Sound Vib.*, vol. 419, pp. 367–379, Apr. 2018.

[16] Y. Liu, J. Liu, W. Chen, and S. Shi, "A U-shaped linear ultrasonic motor using longitudinal vibration transducers with double feet," *IEEE Trans. Ultrason., Ferroelectr., Freq. Control*, vol. 59, no. 5, pp. 981–989, May 2012.

[17] S. Lin and L. Xu, "Study on the radial vibration and acoustic field of an isotropic circular ring radiator," *Ultrasonics*, vol. 52, no. 1, pp. 103–110, Jan. 2012.

[18] J. Melchor and G. Rus, "Torsional ultrasonic transducer computational design optimization," *Ultrasonics*, vol. 54, no. 7, pp. 1950–1962, Sep. 2014.

[19] X. Zhang, S. Lin, Y. Wang, and Z. Fu, "Three-dimensional theory of longitudinal-radial coupled vibration for annular elastic cylinder," *Acta Acustica United Acustica*, vol. 100, no. 2, pp. 254–258, Mar. 2014.

[20] H. Al-Budairi, M. Lucas, and P. Harkness, "A design approach for longitudinal–torsional ultrasonic transducers," *Sens. Actuators A, Phys.*, vol. 198, pp. 99–106, Aug. 2013.

[21] C. Yang, X. Shan, and T. Xie, "A new piezoelectric ceramic longitudinal–torsional composite ultrasonic vibrator for wire drawing," *Ceram. Int.*, vol. 41, pp. 625–630, Jul. 2015.

[22] V. I. Babitsky, V. K. Astashev, and A. N. Kalashnikov, "Autoresonant control of nonlinear mode in ultrasonic transducer for machining applications," *Ultrasonics*, vol. 42, nos. 1–9, pp. 29–35, Apr. 2004.

[23] S. Voronina and V. Babitsky, "Autoresonant control strategies of loaded ultrasonic transducer for machining applications," *J. Sound Vib.*, vol. 313, nos. 3–5, pp. 395–417, Jun. 2008.

[24] S.-H. Wang and M.-C. Tsai, "Dynamic modeling of thickness-mode piezoelectric transducer using the block diagram approach," *Ultrasonics*, vol. 51, no. 5, pp. 617–624, Jul. 2011.

[25] K. Smyth and S.-G. Kim, "Experiment and simulation validated analytical equivalent circuit model for piezoelectric micromachined ultrasonic transducers," *IEEE Trans. Ultrason., Ferroelectr., Freq. Control*, vol. 62, no. 4, pp. 744–765, Apr. 2015.

[26] F. Sammoura and S.-G. Kim, "Theoretical modeling and equivalent electric circuit of a bimorph piezoelectric micromachined ultrasonic transducer," *IEEE Trans. Ultrason., Ferroelectr., Freq. Control*, vol. 59, no. 5, pp. 990–998, May 2012.

[27] H. Zhang, J. Zhao, Y. Hou, J. Zhang, and J. Huang, "A new method to enhance the tip vibration amplitude output of the high frequency piezoelectric ultrasonic transducer used in the thermosonic bonding," *Sens. Actuators A, Phys.*, vol. 294, pp. 116–125, Aug. 2019.

[28] J. Wang and J. Gao, "Numerical value analysis of relationship between resonance frequency of ultrasonic horn and reactive load by numerical calculation," *J. Shaanxi Normal Univ.*, vol. 33, no. 4, pp. 33–35, 2005.

[29] N. Zhang, "Analysis and research on conical load horn," *Acoust. Electr. Eng.*, vol. 2, pp. 30–32, 2007.

[30] J. Ma, B. Zhao, and G. Ren, "Experimental study on the influence of ultrasonic milling tool geometry parameters on acoustic system stability," *Tool Tech.*, vol. 45, no. 6, pp. 50–52, 2011.

[31] H. Ji, W. Yu, and X. Hu, "Influence of force load on resonant frequency and resonant impedance of ultrasonic cutting acoustic system," *J. Vib. Shock*, vol. 35, no. 23, pp. 137–140, 2016.

[32] B. Zhao, W. Bie, X. Wang, F. Chen, Y. Wang, and B. Chang, "The effects of thermo-mechanical load on the vibrational characteristics of ultrasonic vibration system," *Ultrasonics*, vol. 98, pp. 7–14, Sep. 2019.

[33] S. Lin, *Principle and Design of Ultrasonic Transducer*, vol. 3. Beijing, China: Science Press, 2006.

SHUYUAN YE received the M.S. degree in electrical engineering from the Harbin Institute of Technology, Shenzhen, China, in 2018, where he is currently pursuing the Ph.D. degree with the Department of Mechatronics. His current research interests include ultrasonic generator design and control.

JIANZHONG JU received the M.S. degree in mechanical engineering from Northeastern University, Shenyang, China, in 2020. He is currently pursuing the Ph.D. degree with the Department of Mechatronics, Harbin Institute of Technology, Shenzhen, China. His current research interests include ultrasonic machining and ultrasonic assisted friction stir welding.

ZHILI LONG (Member, IEEE) received the B.S., M.S., and Ph.D. degrees in mechatronics engineering from Central South University, Changsha, China, in 2000, 2002, and 2007, respectively.

He is currently an Associate Professor with the Department of Mechatronics, Harbin Institute of Technology, Shenzhen, China. His research interests include modeling and optimization of an ultrasonic actuator.

HENG ZHAO received the M.S. degree in mechanical engineering from Southwest Jiaotong University, Chengdu, China, in 2019. He is currently pursuing the Ph.D. degree with the Department of Mechatronics, Harbin Institute of Technology, Shenzhen, China. His current research interests include ultrasonic transducer design, rotary ultrasonic machining, and advanced manufacture.

YUHUI YANG received the M.S. degree in control engineering from the Harbin Institute of Technology, Shenzhen, China, in 2019. He is currently pursuing the Ph.D. degree with the School of Electromechanical Engineering, Guangdong University of Technology, Guangzhou, China. His current research interests include ultrasonic machining and advanced manufacturing.

• • •